2021-06-15

VEGFC/FLT4-induced cell-cycle arrest mediates sprouting and differentiation of venous and lymphatic endothelial cells

Ayelet Jerafi-Vider
Weizmann Institute of Science

Et al.

Cell Reports

Article

VEGFC/FLT4-induced cell-cycle arrest mediates sprouting and differentiation of venous and lymphatic endothelial cells

Graphical abstract

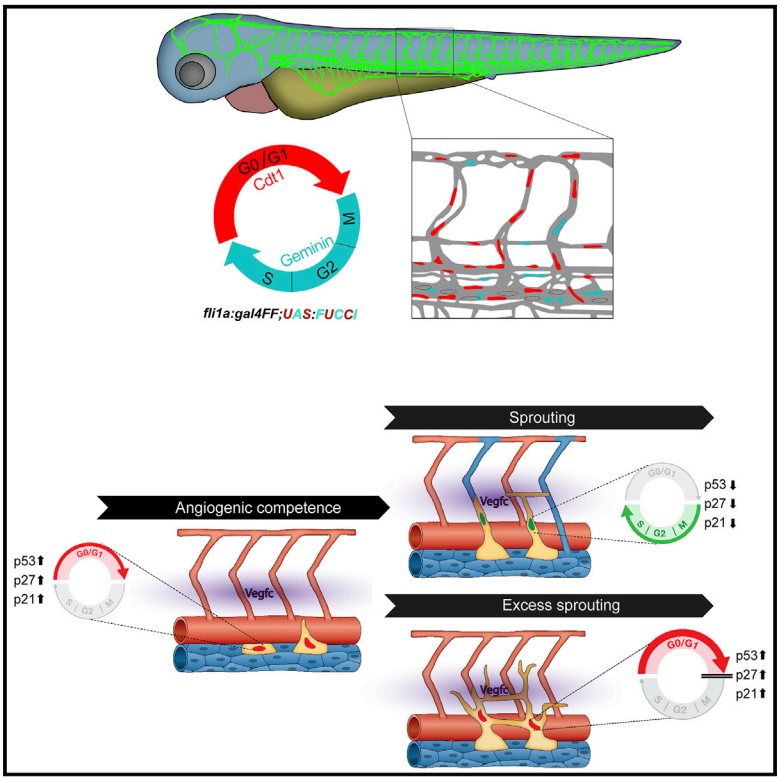

Highlights

- Endothelial cells sprout from the PCV in G1 phase of the cell cycle
- VEGFC/FLT4/ERK induce p53-, p21-, and p27-mediated cell-cycle arrest to enable sprouting
- Forced G1 cell-cycle arrest results in ectopic sprouting of undifferentiated ECs

Authors

Ayelet Jerafi-Vider, Ivan Bassi, Noga Moshe, ..., Masahiro Shin, Nathan D. Lawson, Karina Yaniv

Correspondence

karina.yaniv@weizmann.ac.il

In brief

Jerafi-Vider et al. report a mechanism of endothelial cell sprouting, whereby the mitogenic VEGFC/FLT4/ERK signaling pathway induces p53-, p21-, and p27-mediated cell-cycle arrest, conferring angiogenic potential. These findings have important implications for the putative short-term effects of using cell cycle inhibitors in settings of pathological angiogenesis and lymphangiogenesis.

Jerafi-Vider et al., 2021, Cell Reports *35*, 109255
June 15, 2021
https://doi.org/10.1016/j.celrep.2021.109255

CellPress

Cell Reports

CellPress
OPEN ACCESS

Article

VEGFC/FLT4-induced cell-cycle arrest mediates sprouting and differentiation of venous and lymphatic endothelial cells

Ayelet Jerafi-Vider,[1] Ivan Bassi,[1] Noga Moshe,[1] Yaara Tevet,[1] Gideon Hen,[1] Daniel Splittstoesser,[2] Masahiro Shin,[2] Nathan D. Lawson,[2] and Karina Yaniv[1,3,*]

[1]Department of Biological Regulation, Weizmann Institute of Science, Rehovot 76100, Israel

[2]Department of Molecular, Cell, and Cancer Biology, University of Massachusetts Medical School, Worcester, MA 01605, USA

[3]Lead contact

*Correspondence: karina.yaniv@weizmann.ac.il

https://doi.org/10.1016/j.celrep.2021.109255

SUMMARY

The formation of new vessels requires a tight synchronization between proliferation, differentiation, and sprouting. However, how these processes are differentially activated, often by neighboring endothelial cells (ECs), remains unclear. Here, we identify cell cycle progression as a regulator of EC sprouting and differentiation. Using transgenic zebrafish illuminating cell cycle stages, we show that venous and lymphatic precursors sprout from the cardinal vein exclusively in G1 and reveal that cell-cycle arrest is induced in these ECs by overexpression of p53 and the cyclin-dependent kinase (CDK) inhibitors p27 and p21. We further demonstrate that, *in vivo*, forcing G1 cell-cycle arrest results in enhanced vascular sprouting. Mechanistically, we identify the mitogenic VEGFC/VEGFR3/ERK axis as a direct inducer of cell-cycle arrest in ECs and characterize the cascade of events that render "sprouting-competent" ECs. Overall, our results uncover a mechanism whereby mitogen-controlled cell-cycle arrest boosts sprouting, raising important questions about the use of cell cycle inhibitors in pathological angiogenesis and lymphangiogenesis.

INTRODUCTION

The formation of a new vessel from a pre-existing one requires a tightly regulated synchronization between different processes, such as cell proliferation, specification, and motility (Betz et al., 2016; Marcelo et al., 2013). The balance between cell proliferation and differentiation is considered a hallmark of cell fate determination during embryonic development (Dalton, 2015; Ruijtenberg and van den Heuvel, 2016). In particular, the G1 phase of the cell cycle acts as a critical checkpoint in cell fate decisions, including stem cell differentiation (Calder et al., 2013; Liu et al., 2019). The length of the G1 stage is known to be controlled by cell cycle inhibitors such as p21 and p27, which suppress cyclin/cyclin-dependent kinase (CDK) complex activity (Satyanarayana and Kaldis, 2009; Sherr and Roberts, 1999, 2004). Although the link between cell proliferation and differentiation has been extensively investigated in various embryonic tissues (Dalton, 2015), it is only recently that it attracted attention in the context of vascular formation (Mühleder et al., 2021). Shear stress-dependent upregulation of Notch signaling, for instance, was shown to induce elevation of p27 and blockage of cell cycle in the G1 phase in human umbilical vein endothelial cells (HUVECs), which in turn lead to arterial specification (Fang et al., 2017). Cell proliferation is also tightly linked to angiogenic sprouting. Both in development (Carmeliet et al., 1996; Ferrara et al., 1996) and pathologies (Masood et al., 2001; Millauer et al., 1994), VEGF (vascular endothelial growth factor) stimulates sprouting and growth of endothelial cells (ECs) and formation of new blood vessels, acting mainly through its receptor VEGFR2. Surprisingly however, a recent report demonstrated that high levels of VEGF-A in fact inhibited the proliferation of tip cells in the postnatal mouse retina, while promoting their active migration and sprouting (Pontes-Quero et al., 2019). In contrast to these advances, little is known about the spatiotemporal dynamics of cell cycle progression in ECs *in vivo* and how it affects angiogenesis and sprouting. Moreover, whether cell cycle progression is linked to the initial venous EC (VEC) versus lymphatic EC (LEC) segregation has not been addressed.

During embryonic development, VECs and LECs sprout from the cardinal vein (CV) toward a gradient of VEGFC (Karkkainen et al., 2004; Semo et al., 2016). Accordingly, VEGFC-deficient mice and zebrafish fail to establish a proper lymphatic system (Gancz et al., 2019; Jeltsch et al., 1997; Karkkainen et al., 2004; Küchler et al., 2006; Villefranc et al., 2013; Yaniv et al., 2006). VEGFR3 (also known as Flt4) is the main receptor for VEGFC, and its activation mediates LEC proliferation, migration, and survival (Kaipainen et al., 1995; Mäkinen et al., 2001; Tammela et al., 2008). In zebrafish, mutations in *vegfr3* result in the complete absence of the lymphatic vasculature and defective venous sprouting, without affecting arterial development (Gancz et al., 2019; Hogan et al., 2009a; Kok et al., 2015). In addition to its mitogenic role, the Vegfc-Flt4 signaling axis has also been

shown to promote differentiation and sprouting of lymphatic progenitors from the posterior CV (PCV) in zebrafish embryos, through ERK (extracellular signal-regulated kinase) activation (Deng et al., 2013; Shin et al., 2016). Nevertheless, how the processes of EC proliferation, cell fate specification (i.e., venous versus lymphatic), and sprouting are orchestrated during embryonic development to enable two different vessel types to arise almost simultaneously from the PCV remains largely unknown.

Here, we investigate the link between cell cycle progression, differentiation, and sprouting of VECs and LECs emerging from the PCV of the zebrafish embryo. Using live imaging of transgenic reporters highlighting different stages of the cell cycle, we show that both VECs and LECs bud from the dorsal side of the PCV in G1 phase and demonstrate that cell-cycle arrest is specifically induced in these "angiogenic" ECs through upregulation of p53, p21, and p27. Using chemical and genetic manipulations, we further reveal that induction of cell-cycle arrest in PCV ECs results in excessive sprouting of undifferentiated ECs from the PCV. Molecularly, we identify the Vegfc-Flt4 signaling axis as a regulator of p53, p21, and p27 expression in angiogenic ECs and characterize the cascade of downstream events orchestrating the segregation of venous and lymphatic vessels. Overall, our results uncover an additional layer of regulation of sprouting angiogenesis whereby arresting cell cycle progression at the G1 phase promotes vessel sprouting, raising important questions about the role of cell cycle inhibitors in states of pathological angiogenesis.

RESULTS

ECs sprout from the PCV in G1 phase

To investigate the link between cell cycle progression and EC sprouting *in vivo*, we established *Tg(fli1a:Gal4FF;UAS:FUCCI)* transgenic fish (Figure 1A) in which EC nuclei in late G1 are labeled in red (mCherry), and those in S/G2/M phases display cerulean fluorescence (Fukuhara et al., 2014; Sugiyama et al., 2009). By mating these fish with *Tg(kdrl:tagBFP)* (Matsuoka et al., 2016) animals, which feature non-nuclear, blue fluorescence in all ECs, we can distinguish ECs not labeled by either *FUCCI* fluorophore, by virtue of cytoplasmically expressed *tagBFP* (Figures 1B and 1D). Based on previous reports using FUCCI (Canu et al., 2020; Pauklin and Vallier, 2013), such cells (i.e., *tagBFP+;FUCCI−*) are expected to be in early G1. Confocal imaging of *Tg(fli1a:Gal4FF;UAS:FUCCI;kdrl:tagBFP)* embryos revealed significant changes in the cell cycle phase distribution of PCV-ECs, between 26 and 42 hours post-fertilization (hpf). While the relative number of late G1 cells (*mCherry+*) increased from 28% to 67% (Figures 1B, 1C, and 1F; Figure S1A), that of S/G2/M cells (*cerulean+*) dramatically declined (Figure S1A). Accordingly, we detected an overall reduction in the total number of PCV-ECs between 26 to 42 hpf (Figure S1B). Alongside the cell cycle allocation changes, we observed significant differences in the spatial distribution of late-G1 ECs between these two time points. Slightly before the initiation of lympho-venous sprouting (~26 hpf), late G1 cells were evenly distributed throughout the PCV (Figures 1B, 1C, and 1G). In contrast, during stages of active sprouting (42 hpf), ~74% of the late-G1 cell population was restricted to the dorsal side of the PCV (Figures 1D, 1E, and 1G). We used long-term time-lapse imaging of Tg(*fli1a:Gal4FF;UAS:FUCCI;UAS:Kaede)* embryos to track the dynamics of cell cycle progression during PCV sprouting (Figures 1H–1O; Figure S1C; Video S1). We observed that ECs bud from the PCV in late-G1 phase (red), and upon crossing the anatomical level of the dorsal aorta (DA), the *mCherry* signal rapidly declines (Figures 1K and 1N, purple arrowheads; Figure S1C). This process was independent of whether the sprouting cell was a venous EC giving rise to a venous intersegmental vessel (vISV) (Figures 1H–1K; Figures S1C and S1D) or a lymphatic progenitor incorporating into the parachordal chain (PAC) (Figures 1L–1O; Figures S1C and S1D). These observations demonstrate a correlation between late G1 arrest and the sprouting of ECs from the PCV.

Each phase of cell cycle progression is driven by specific CDKs and their cyclin binding partners. To coordinate these phases, cyclin-CDK inhibitors (CKIs), including p27 and p21, negatively regulate CDK activity and cell cycle progression (Satyanarayana and Kaldis, 2009), inducing growth arrest at the G0/G1 checkpoint. Upstream of CKIs are tumor suppressors, such as p53, which can promote G0/G1 cell-cycle arrest in part by inducing CKI expression. Based on our observations above, we analyzed the expression of p53, p27, and p21 in 30- and 48-hpf (i.e., stages of active PCV sprouting) *Tg(fli1:EGFP)* embryos. Interestingly, we detected expression of *p21* mRNA in the PCV of 24-hpf embryos (Figure S1E) as well as accumulation of p53 (Figures 1P, 1Q, and 1T, blue arrowheads) and p27 (Figures 1R, 1S, and 1U, blue arrowheads) proteins in ECs located in the dorsal PCV. The p53 protein was also detected in intersomitic vessels (ISVs), which at this time have arterial identity (Figures 1P and 1Q, white arrowheads; Isogai et al., 2003). Taken together, these results suggest an important role of p53, CKIs, and cell-cycle arrest in sprouting of lympho-venous cells from the PCV.

p53, p21, and p27 mediate G1 cell-cycle arrest in sprouting PCV ECs

To investigate a functional connection between cell-cycle arrest and PCV sprouting, we first treated *fli:FUCCI* embryos with roscovitine, a broad CDK inhibitor that can induce cell-cycle arrest in G1 (Alessi et al., 1998; Lee et al., 2008; Lu et al., 2001). The treatment was initiated at 20 hpf, before the onset of PCV sprouting, in order to avoid potential non-specific effects derived from defects in arterial ISV formation, which takes place earlier. As expected, roscovitine treatment of *fli1:fucci* embryos resulted in increased numbers of late-G1 mCherry+ ECs that were evenly distributed in the PCV of treated embryos by 48 hpf (Figures 2A–2C). Consistent with a pro-angiogenic role for G1 arrest, we observed evidence of excessive angiogenic behaviors, including significant incidence of ectopic sprouts emanating from the PCV, induced by roscovitine compared to DMSO-treated siblings (Figures 2D–2F; Video S2). Notably, roscovitine treatment did not affect the expression levels of *vegfc* or *flt4* mRNAs at 26 hpf (Figures S2A and S2B), excluding the increased expression of these two factors as a reason for the observed excess sprouting phenotype. We found a similar effect in embryos treated with flavopiridol, a

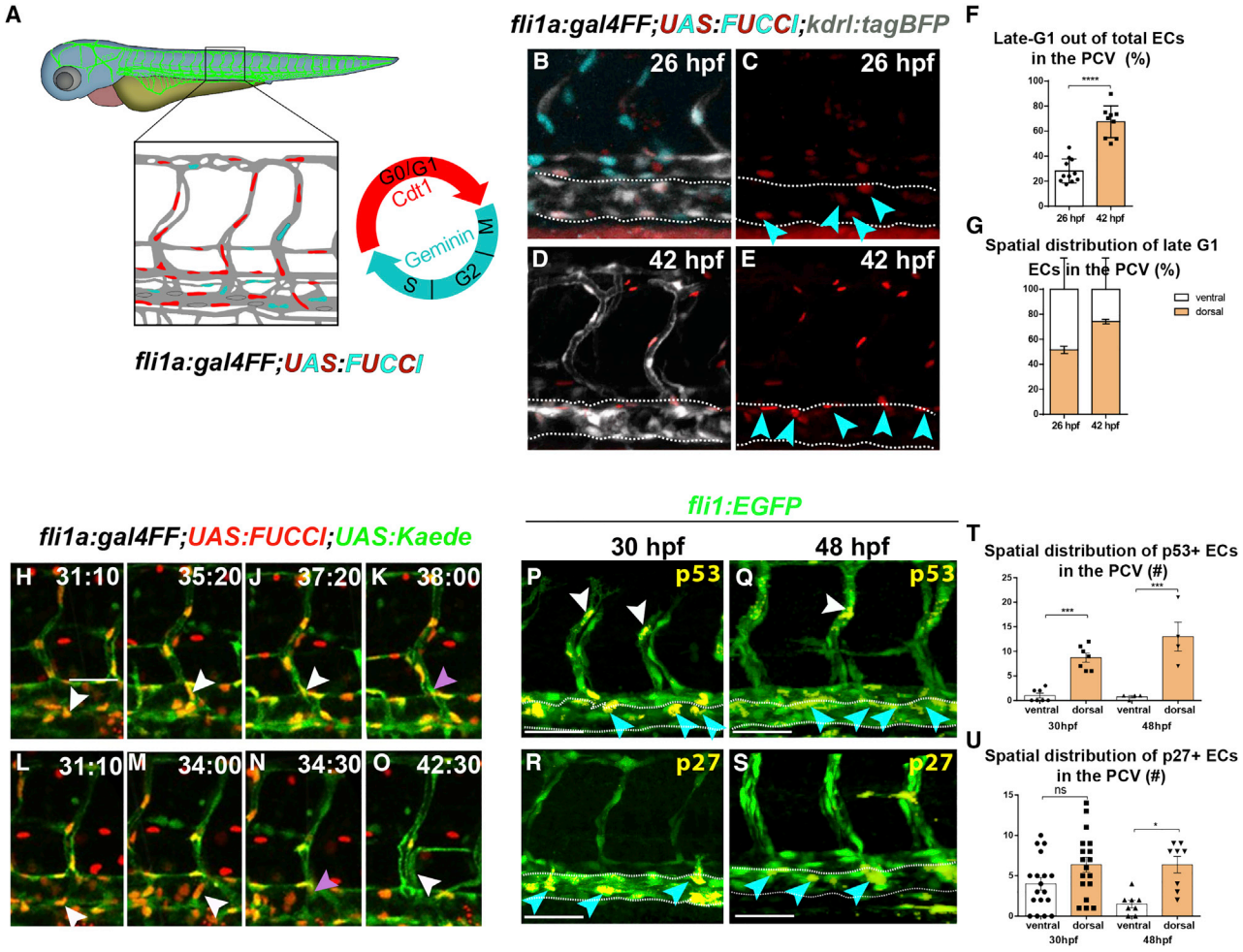

Figure 1. Endothelial cells sprout from the PCV in G1 phase

(A) Schematic representation of cell cycle stages in ECs as highlighted by the *Tg(fli1a:Gal4FF;UAS:FUCCI)* reporter.

(B–E) Selected confocal snapshots from a time-lapse series of a *Tg(fli1a:Gal4FF;UAS:FUCCI;kdrl:tagBFP)* embryo depicting the distribution of late G1 (red) ECs in the PCV (outlined by dashed lines) at 26 (B and C, light-blue arrowheads) and 42 (D and E, light-blue arrowheads) hpf.

(F) Fraction of late-G1 ECs out of total PCV cells ($n_{26\ hpf\ embryos}$ = 11; $n_{42\ hpf\ embryos}$ =9). Data show mean ± SEM (unpaired t test).

(G) Spatial distribution of late-G1 ECs in the PCV at 26 and 42 hpf ($n_{26\ hpf\ embryos}$ = 11; $n_{42\ hpf\ embryos}$ =9). Data show mean ± SEM (unpaired t test).

(H–O) Selected snapshots from a time-lapse series of a *Tg(fli1a:Gal4FF;UAS:FUCCI;UAS:Kaede)* embryo showing two different ECs budding off the PCV in late-G1 stage (H and L, white arrowheads) and re-entering cell cycle upon crossing the DA (K and N, purple arrowhead).

(P–S) Confocal images of 30 (P and R) and 48 (Q and S) hpf *Tg(fli1:EGFP)* embryos immuno-stained with p53 (P and Q, light-blue arrowheads) or p27 (R and S, light-blue arrowheads) antibodies. Co-localization channel is shown in yellow, and PCV is outlined by dashed lines.

(T and U) Spatial distribution of p53+ ($n_{30\ hpf}$ = 7, $n_{48\ hpf}$ = 4) (T) and p27+ ($n_{30\ hpf}$ = 18, $n_{48\ hpf}$ = 8) (U) ECs in the PCV. Data show mean ± SEM (one-way ANOVA plus Tukey's post-hoc test). Scale bars: 40 μm (B–E and H–O), 70 μm (P–S); *p < 0.05, ***p < 0.001, ****p < 0.0001; ns, not significant.

potent CDK inhibitor that can also induce G1 arrest, which is clinically efficient for cancer treatment (Carlson et al., 1996, Senderowicz, 1999) (Figure 2G, white arrowheads; Figure S2A, light-blue arrowheads). In contrast, treatment with inhibitors known to interfere with other cell cycle phases, such as aphidicolin (S), nocodazole (M), or etoposide (G2), failed to induce ectopic sprouting (Figures 2H–2J). We noted that both aphidicolin (Figure 2H) and nocodazole (Figure 2I) treatments resulted in severe vascular defects, albeit they elicited different effects on S/G2/M (cerulean+) cells (Figure S2C).

In addition to promoting cell-cycle arrest through CKI inhibition, both flavopiridol and roscovitine can stabilize p53 by inhibiting CDK9-mediated elongation of transcripts encoding MDM2 and MDM4, which normally contribute to p53 degradation (Lu et al., 2001; Štětková et al., 2020). Stabilization of p53 in this setting then contributes to cell-cycle arrest by inducing expression of CDKIs, such as p21. To determine if this mechanism contributed to ectopic sprouting from the PCV, we treated embryos homozygous for a tp53 point mutation (*tp53*^{M214K}) that prevents its ability to bind to DNA and induce target genes

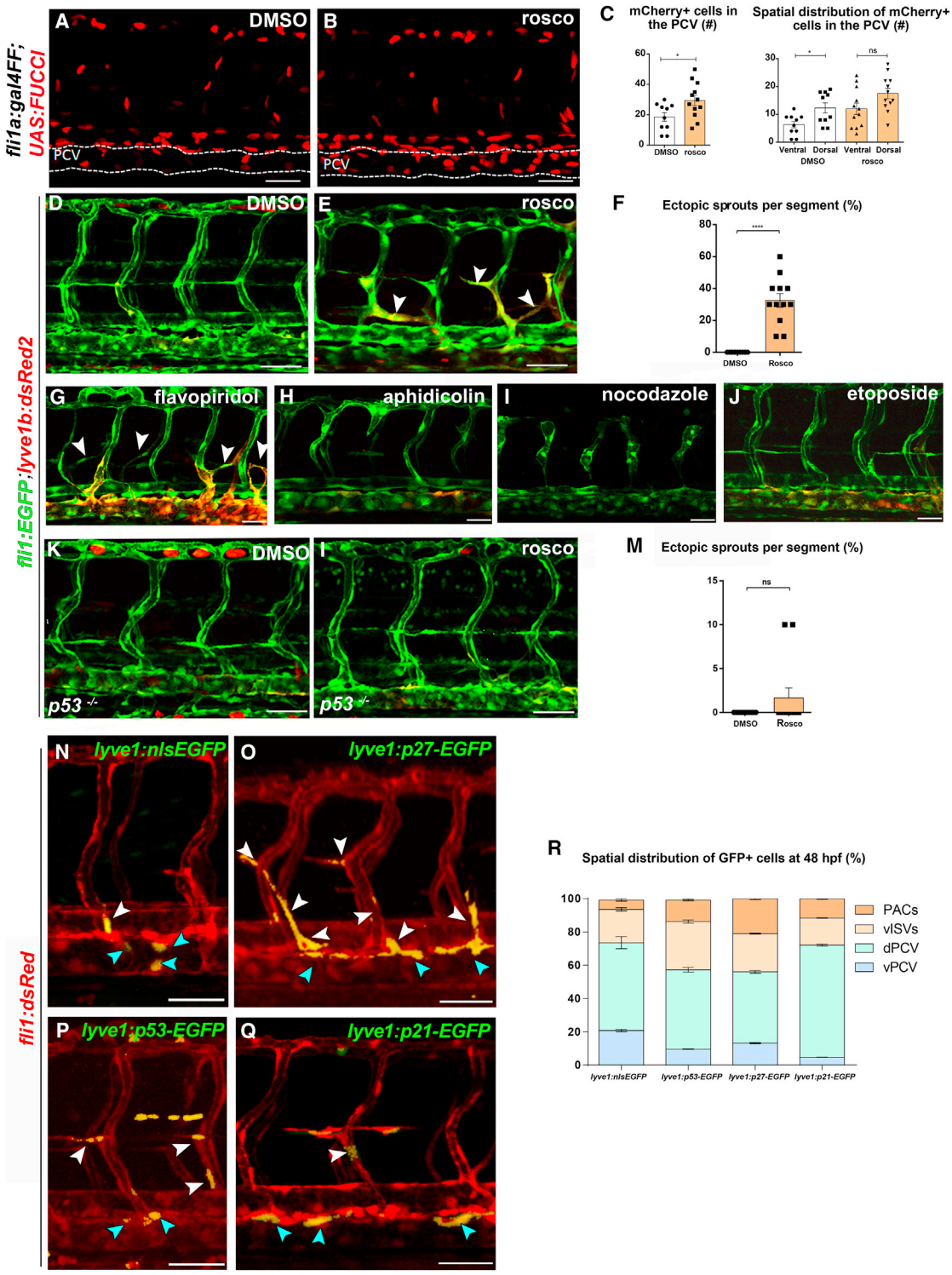

Figure 2. G0/G1 cell-cycle arrest in PCV ECs is mediated by p53, p21, and p27

(A–C) Confocal images of *Tg(fli1a:Gal4FF;UAS:FUCCI)* (red channel) embryos at 48 hpf, showing increased numbers of late-G1 *mCherry+* nuclei, which are evenly distributed throughout the PCV (outlined by dashed lines) following roscovitine versus DMSO treatment (A and B); quantified in (C) (n_{DMSO} = 10, n_{rosco} = 12). Data show mean ± SEM (unpaired t test).

(D and E) Confocal images of 48-hpf *Tg(fli1:EGFP;lyve1b:dsRed2)* embryos showing ectopic and mis-patterned PCV sprouts following roscovitine treatment (E, arrowheads), which are not detected in DMSO-treated siblings (D).

(legend continued on next page)

(Berghmans et al., 2005). Unlike wild-type (WT) animals, roscovitine-treated *p53* mutants did not display a significant increase in ectopic sprouting (Figures 2K–2M), suggesting that p53 is largely responsible for driving cell-cycle arrest and subsequent sprouting following roscovitine treatment.

As noted above, roscovitine likely has multiple mechanisms of action and its effects are not limited to ECs. Therefore, to specifically manipulate cell cycle in a cell autonomous manner, we overexpressed EGFP-tagged p53, p21, or p27 in the PCV of *Tg(fli1:dsRed)* and of *Tg(fli1a:Gal4FF;UAS:FUCCI)* embryos by using the *lyve1* promoter (Okuda et al., 2012) and analyzed the behavior of the labeled cells at 48 hpf. A *lyve1:nlsEGFP* plasmid was used as a control. As seen in Figures 2N–2R, *lyve1* drove transgene expression as expected in the PCV and in venous and lymphatic sprouts at 48 hpf. Moreover, the vast majority of PCV ECs expressing p21-GFP or p27-GFP were also labeled by mCherry in *fli:fucci* embryos, indicating that these cells were in the G1 phase of the cell cycle (Figures S2E and S2F). Interestingly, an assessment of the spatial distribution of the EGFP+ ECs revealed significant differences between the injected groups. Although only 25.66% of EGFP+ cells were detected outside the PCV (i.e., in vISVs and PACs) in control-injected embryos (Figures 2N and 2R), almost twice the amount (41.92% and 43.87%) was observed in venous and lymphatic sprouts following overexpression of p53 and p27, respectively (Figures 2O, 2P, and 2R, white arrows). In addition, there was a significant shift of EGFP+ cells from the ventral to the dorsal side of the PCV (Figures 2O and 2P, light-blue arrows), suggesting that p53 and p27 act cell autonomously in ECs to induce sprouting. Unlike p53- and p27-overexpressing embryos, *lyve1:p21-EGFP*-injected larvae survived through adulthood and were fertile, enabling the generation of stable transgenic animals and assessment of the spatial distribution of EGFP+ cells in their progeny at 48 hpf. Notably, the vast majority of the EGFP+ cells in *p21*-overexpressing embryos was detected in the dorsal PCV (67.44%) and in lymphatic/venous sprouts (27.9%), as opposed to only 4.65% that were found in the ventral PCV (Figures 2Q and 2R). Taken together, these results indicate that the increased expression of p53, p27, and p21 acts cell autonomously in PCV ECs to promote cell-cycle-arrest-induced sprouting.

Cell-cycle arrest in dorsal PCV ECs is VegfC/VegfR3 dependent

During embryonic development, venous and lymphatic ECs sprout from the CV in response to Vegfc-Vegfr3 signaling (Petrova and Koh, 2018; Semo et al., 2016). In zebrafish, Vegfc is expressed in the hypochord and the DA (Cohen et al., 2020; Covassin et al., 2006; Hogan et al., 2009b), whereas its receptor, Flt4, is expressed in PCV ECs, including those in lymphatic and venous sprouts. Mutations in either *vegfc* or *flt4* lead to a block in sprouting of lymphatic and venous ECs from the PCV and a failure to develop a functional lymphatic system, along with defective arteriovenous remodeling of ISVs (Covassin et al., 2006; van Impel et al., 2014; Siekmann and Lawson, 2007).

To determine a potential connection between Vegfc/Flt4 signaling and cell cycle, we first assessed p27 and p53 levels in *vegfc* (Villefranc et al., 2013) and *flt4* (Shin et al., 2016) mutants. Immunostaining revealed a significant reduction in the number of p27- and p53-expressing ECs in the PCV of embryos mutant for either *flt4* or *vegfc* when compared to WT siblings (Figures 3A–3G, light-blue arrowheads; Figures S3A–S3F). Thus, induction of p27 and p53 expression is dependent on Vegfc signaling. Based on this finding, we next determined whether restoring the expression of p53, p27, or p21 can rescue lympho-venous sprouting. Interestingly, we observed a modest but significant increase in the number of incipient sprouts arising from the PCV in *flt4* and *vegfc* mutants injected with *lyve1:p27-EGFP* (Figures 3H–3K, white arrowheads; Figure 3N). Although a similar trend was noted with *lyve1:p53-EGFP* (Figures 3L and 3M, white arrowheads), this was not statistically significant (Figure 3N). In contrast, p21 did not appear to have any effect (Figure 3N). Despite the increased number of emerging sprouts induced by p27 and, to a lesser extent, by p53 in the absence of Vegfc or Flt4, we noted that these sprouts failed to elongate past the level of the DA (Figures 3H–3M). In contrast, WT intersomitic venous vessels are fully formed at this stage and have reached the level of the dorsal longitudinal anastomotic vessel (DLAV; e.g., see Figure 2D). These observations suggest that, although cell-cycle arrest alone is sufficient to enable the budding and angiogenic behavior of PCV-ECs, it cannot fully rescue the loss of Vegfc/Flt4 signaling. Accordingly, we find that the hyperangiogenic response induced by roscovitine is likewise eliminated in embryos mutant for *flt4* or *vegfc* (Figures 3O–3U). Hence, it appears that parallel Vegfc/Flt4-activated pathways are needed in order to facilitate the dorsal migration of emerging PCV-ECs.

Our results suggest that distinct signals downstream of Vegfc/Flt4 likely promote migration and cycle arrest. Among the functional effectors of Vegfc/Flt4 activation is ERK, which is required for lympho-venous sprouting and induction of lymphatic specification. To determine if ERK might be in a pathway common to cell-cycle arrest, we used a well-known selective inhibitor of MEK1/2, SL327, which blocks ERK phosphorylation and

(F) Number of ectopic sprouts per segment in roscovitine- versus DMSO-treated embryos (n_{DMSO} = 11, n_{rosco} = 12). Data show mean ± SEM (unpaired t test).
(G–J) Confocal images of 3-dfp *Tg(fli1:EGFP;lyve1b:dsRed2)* embryos treated with flavopiridol (J, n = 14), aphidicolin (G, n = 6), nocodazole (H, n = 11), or etoposide (I, n = 11), showing ectopic and mis-patterned PCV sprouts following flavopiridol treatment (J, arrowheads).
(K and L) Confocal images of *Tg(fli1:EGFP;lyve1b:dsRed2;p53$^{-/-}$)* embryos at 48 hpf, showing normal PACs following DMSO (K) and roscovitine (L, arrowheads) treatments.
(M) Percentage of ectopic sprouts per segment in roscovitine-treated (n = 12) versus DMSO-treated (n = 12) *p53$^{-/-}$* embryos. Data show mean ± SEM (unpaired t test).
(N–P) Confocal images of *Tg(fli1:DsRed)* embryos 48 after injection with *lyve1:nEGFP* (N, n = 12), *lyve1:p27-EGFP* (O, n = 12), or *lyve1:p53-EGFP* (P, n = 30).
(Q) Confocal images of *Tg(fli1:DsRed;lyve1:p21-EGFP)* embryos at 48 hpf. Light-blue arrowheads in (N)–(Q) point to GFP+ ECs in the dorsal PCV, white arrowheads denote GFP+ lymphovenous sprouts, and co-localization channel is shown in yellow.
(R) Spatial distribution of GFP+ cells in *lyve1:nEGFP-*, *lyve1:p27-EGFP-*, *lyve1:p53-EGFP-*, and *lyve1:p21-EGFP*-expressing embryos. Scale bars: 40 μm (A–L), 50 μm (N–Q). *p < 0.05, ****p < 0.0001; ns, not significant.

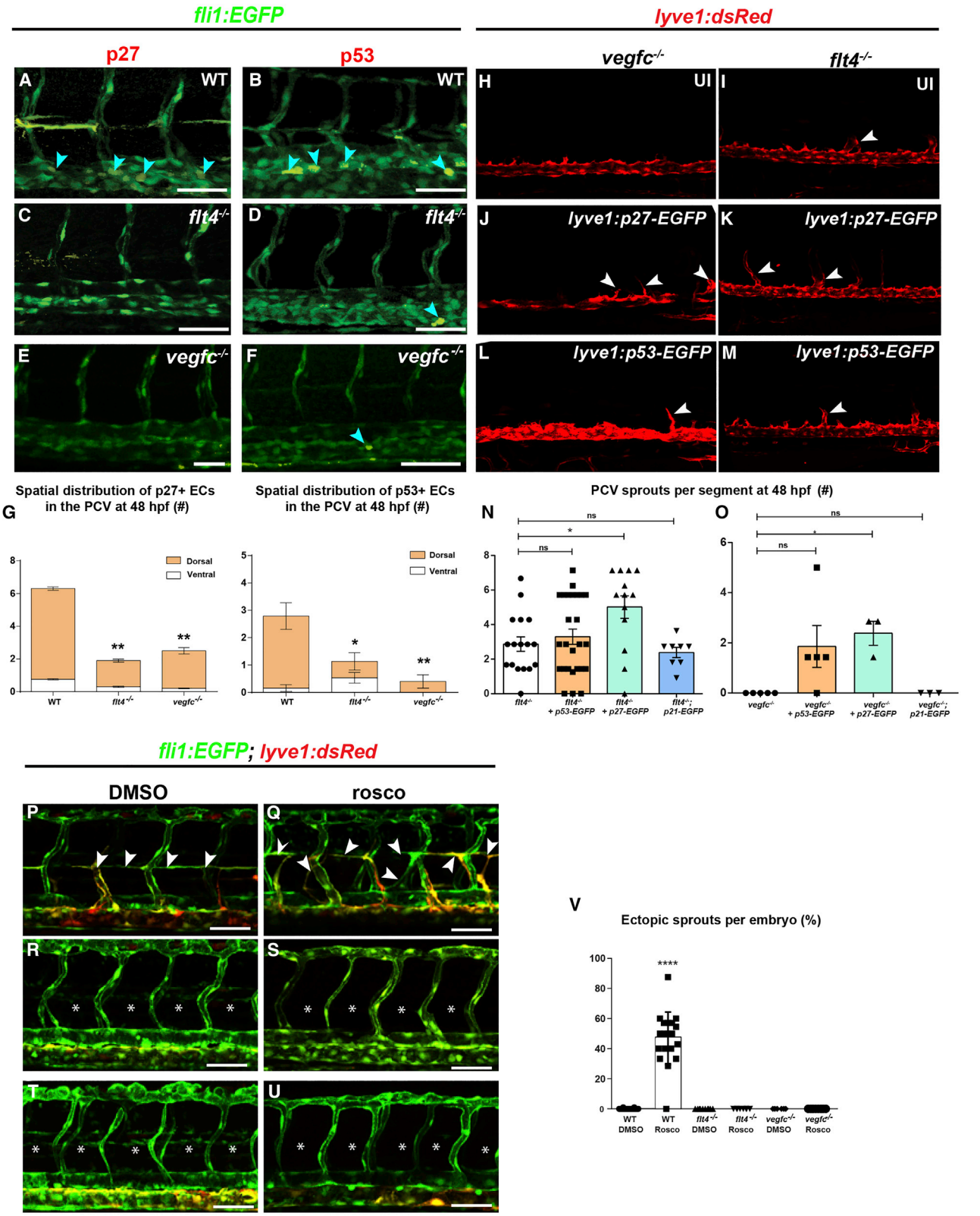

(legend on next page)

downstream signaling (Shin et al., 2016). Treatment of zebrafish embryos with SL327 at 24 hpf was shown to inhibit both venous and lymphatic sprouting (Shin et al., 2016). We treated 20-hpf *fli:fucci* and *Tg(mrc1a:EGFP)* (Jung et al., 2017) embryos with either roscovitine or DMSO, then added SL327 at 24 hpf, and analyzed PCV sprouting 1 day later. Interestingly, both pharmacological inhibitors promoted G1 arrest, as confirmed by the increased number of red nuclei detected in treated *fli:fucci* embryos as compared to their DMSO-treated siblings (Figures S4A–S4E). Despite this common cellular effect, roscovitine induced excessive PCV sprouting (Figures 4A, 4B, and 4E), whereas SL327 potently blocked the emergence of venous and lymphatic sprouts from the PCV (Figures 4A, 4C, and 4E). However, the combination of roscovitine and SL327 treatments resulted in a more robust rescue of PCV sprouting (Figures 4C, 4D, and 4E) than what we observed in *vegfc* and *flt4* mutants, suggesting that p53/p21-mediated G1 cell-cycle arrest may be induced downstream of ERK signaling to enable PCV sprouting. Further supporting this conclusion, ERK phosphorylation in the PCV remained unchanged following roscovitine treatment (Figures S4F–S4I). In addition to roscovitine, stable overexpression of p21 in *Tg(fli:DsRed;lyve1:p21-EGFP)* embryos (Figures 4F–4I and 4L), as well as transient overexpression (OE) of p53 through injection of *lyve1:p53-EGFP* (Figures 4F, 4G, 4J, and 4L), was sufficient to induce PCV sprouting in the absence of active MEK signaling, whereas *lyve1:p27-EGFP* was not able to overcome the SL327-induced effects (Figures 4G, 4K, and 4L). Finally, the expression of both p53 and p27 was significantly reduced in SL327-treated embryos (Figures 4M–4P). Taken together, these results suggest that Vegfc/Flt4 signaling through ERK is required to drive the observed cell-cycle arrest during PCV sprouting. However, parallel pathways, also stimulated by Vegfc/Flt4 activation, including other targets of ERK, are essential for subsequent EC migration and sprout elongation.

Forced G0/G1 cell-cycle arrest affects venous-lymphatic differentiation

Given that the VegfC-VegfR3-ERK cascade was found to control not only venous and lymphatic sprouting but also lymphatic specification (Deng et al., 2013; Shin et al., 2016; Yu et al., 2014), we decided to investigate whether cell cycle progression also plays a role in this process. We began by analyzing the expression of venous and lymphatic markers following roscovitine treatment (Figure 5). *In situ* hybridization at 24 and 30 hpf revealed a significant decrease in *lyve1* and *nr2f2* mRNA expression in treated embryos (Figures 5A and 5B), whereas the expression of the venous-specific *ephb4a* marker remained unchanged. Furthermore, the number of *prox1*+ cells detected in the PCV of roscovitine-treated *Tg(fli1:EGFP;prox1a:KalTA4-4xUAS-E1b:uncTagRFP)* (Nicenboim et al., 2015) embryos was significantly decreased as compared to DMSO-treated siblings (Figures 5D–5F; Figures S4J and S4K), indicating that forced cell-cycle arrest inhibits the segregation of lymphatic progenitors within the PCV, while promoting their exit and sprouting. To better understand this phenotype, we time-lapse imaged *Tg(fli1:EGFP)* embryos continuously exposed to roscovitine and tracked the behavior of ECs sprouting from the PCV. As seen in Figures 5G–5L and Video S3, we detected single sprouts for which the leading cell (colored in red) connects to a neighboring arterial ISV to generate a lumenized vISV;however, the following cell (colored in blue) divides horizontally and generates two daughter cells, with one of them incorporating into the PAC and the other joining a vISV. This phenotype of undifferentiated PCV cells generating both venous and lymphatic cells after sprouting is rarely observed in WT embryos (Geudens et al., 2019), because for the most part, lymphatic progenitors have been shown to acquire their fate prior to leaving the PCV (Koltowska et al., 2015; Nicenboim et al., 2015).

Altogether, our results illustrate how different signaling pathways are exquisitely synchronized both in time and space to support proper angiogenesis and lymphangiogenesis in the developing embryo and introduce a level of regulation to this process involving cell-cycle arrest (Figure 5M). Based on our findings, we propose that distinct levels of VegfC/Flt4 signaling control sprouting and differentiation of PCV-ECs, through parallel, ERK-dependent and independent mechanisms. Differentiated venous and lymphatic ECs located in the dorsal side of the PCV are exposed to high levels of the VegfC ligand, which is secreted from the hypochord and the DA. In these cells, ERK signaling (most likely of high magnitude and prolonged activation) induces the expression of p53 and p21 to enable sprouting. Concordantly, both roscovitine treatment and cell-autonomous overexpression of p21 and p53 were sufficient to partially overcome the inhibition

Figure 3. Cell-cycle arrest in dorsal PCV ECs is VegfC/VegfR3 dependent

(A–F) Confocal images of 48-hpf WT (A and B), *flt4*$^{-/-}$ (C and D), and *vegfc*$^{-/-}$ (E and F); *Tg(fli1:EGFP)* embryos, stained with p27 (A, C, and E) or p53 (B, D, and F) antibodies. Light-blue arrowheads point to immunostained ECs, and co-localization channel is shown in yellow.

(G) Number and spatial distribution of p27- and p53-stained ECs, in the PCV of WT, *flt4*$^{-/-}$, and *vegfc*$^{-/-}$; *Tg(fli1:EGFP)* embryos ($n_{p27\ wt}$ = 19, $n_{p27\ flt4-/-}$ = 8, $n_{p27\ vegfc-/-}$ = 10, $n_{p53\ WT}$ = 17, $n_{p53\ flt4-/-}$ = 15, $n_{p53\ vegfc-/-}$ = 5). Statistical analysis was performed using one-way ANOVA followed by Tukey's multiple comparisons test.

(H–M) Confocal images of 48-hpf *vegfc*$^{-/-}$ (H, J, and L) and *flt4*$^{-/-}$ (I, K, and M); *Tg(lyve1b:dsRed2)* embryos, uninjected (H and I, $n_{vegfc-/-}$ = 5, $n_{flt4-/-}$ = 17) or injected with *lyve1:p27-EGFP* (J and K) or *lyve1:p53-EGFP* (L and M). White arrowheads point to PCV emerging sprouts.

(N) Number of ectopic sprouts per segment in *flt4*$^{-/-}$;*Tg(lyve1b:dsRed2)* embryos injected with *lyve1:p27-EGFP* (n = 13) or *lyve1:p53-EGFP* (n = 26) or stably expressing *lyve1:p21-EGFP* (n = 8). Statistical analysis was performed using Kruskal-Wallis followed by Dunnett's multiple comparisons test.

(O) Number of ectopic sprouts per segment in *vegfc*$^{-/-}$;*Tg(lyve1b:dsRed2)* embryos injected with *lyve1:p27-EGFP* (n = 3) or *lyve1:p53-EGFP* (n = 5) or stably expressing *lyve1:p21-EGFP* (n = 3). Statistical analysis was performed using Kruskal-Wallis followed by Dunnett's multiple comparisons test.

(P–V) Confocal images of WT (P and Q), *flt4*$^{-/-}$ (R and S), and *vegfc*$^{-/-}$ (T and U); *Tg(fli1:EGFP;lyve1b:dsRed2)* embryos at 3 days post-fertilization (dpf), treated with DMSO (n_{WT} = 24, $n_{flt4-/-}$ = 10, $n_{vegfc-/-}$ = 6) or roscovitine (n_{WT} = 19, $n_{flt4-/-}$ = 8, $n_{vegfc-/-}$ = 10). Statistical analysis was performed using one-way ANOVA followed by Tukey's multiple comparisons test. White arrowheads in (P) and (Q) point to normal and ectopic lymphovenous sprouts that are absent in *flt4* and *vegfc* mutants (R–U, asterisks); quantified in (V). *p < 0.05, ***p < 0.001, ****p < 0.0001; ns, not significant. Scale bars: 70 μm.

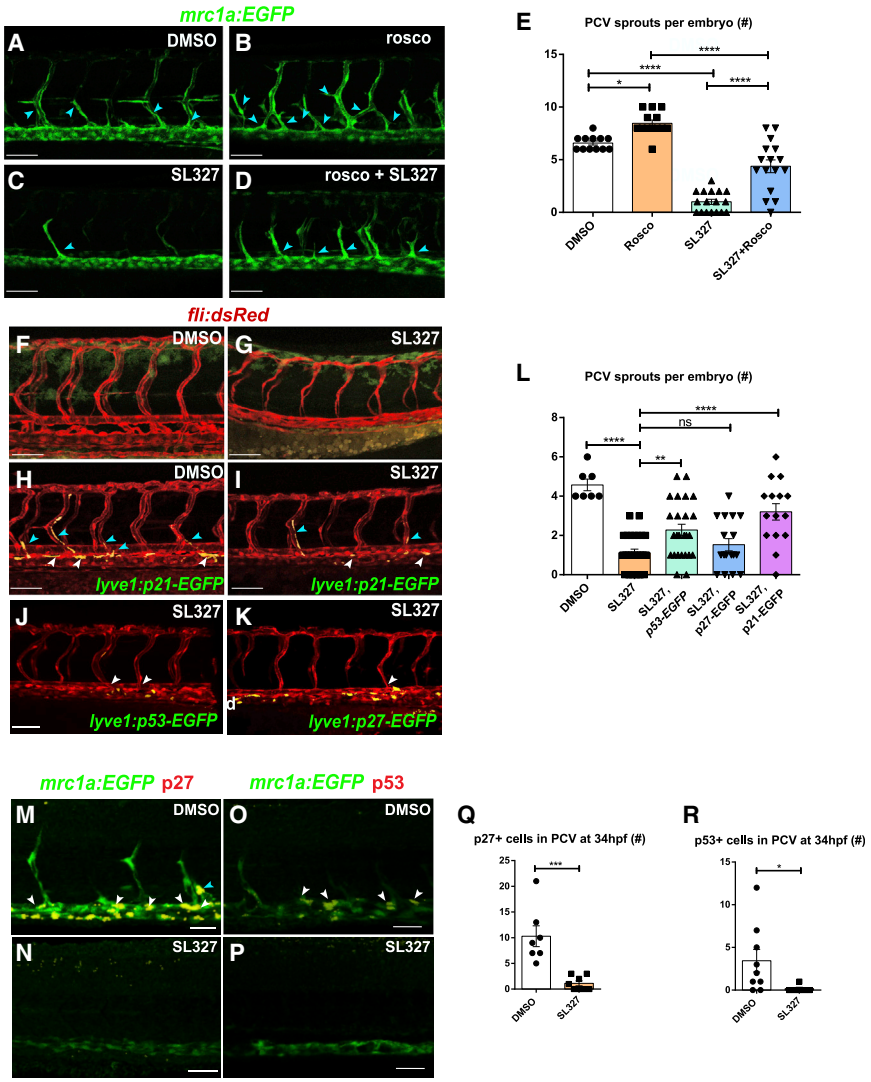

Figure 4. Cell-cycle arrest acts downstream to ERK signaling in PCV ECs

(A–E) Confocal images of 48-hpf *Tg(mrc1a:EGFP)* embryos treated with DMSO (A), roscovitine (B), SL327 (C), or roscovitine+SL327 (D) showing partial rescue of lymphovenous sprouting following roscovitine + SL327 (D) treatment, and quantified in (E) (n_{DMSO} = 12, n_{rosco} = 13, n_{SL327} = 17, $n_{rosco+SL327}$ = 16). Statistical analysis was performed using one-way ANOVA followed by Tukey's multiple comparisons test. Blue arrowheads in (A)–(D) point to PCV sprouts.

(F–L) Confocal images of *Tg(fli1:dsRed2)* embryos treated with DMSO (F and H) or SL327 (G, I, J, and K) stably expressing *lyve1:p21-EGFP* (H and I) or injected with *lyve1:p53-EGFP* (J) or *lyve1:p27-EGFP* (K), showing partially restored lymphovenous sprouting, and quantified in (L) (n_{DMSO} = 7, n_{SL327} = 26, $n_{lyve1:p21-EGFP+DMSO}$ = 7, $n_{lyve1:p21-EGFP+SL327}$ = 15, $n_{lyve1:p27-EGFP+SL327}$ = 17, $n_{lyve1:p53-EGFP+SL327}$ = 25). Statistical analysis was performed using one-way ANOVA followed by Tukey's multiple comparisons test. Light-blue arrowheads in (H)–(K) point to GFP+ ECs in the dorsal PCV, white arrowheads denote GFP+ lymphovenous sprouts, and co-localization channel is shown in yellow.

(M–P) Confocal images of 34-hpf *Tg(mrc1a:EGFP)* embryos showing reduced expression of p27 (M and N) and p53 (O and P) following SL327 treatment, and quantified in (Q and R) ($n_{DMSO\ p27}$ = 7, $n_{SL327\ p27}$ = 8, $n_{DMSO\ p53}$ = 9, $n_{SL327\ p53}$ = 6). Data show mean ± SEM (unpaired t test). Co-localization channel is shown in yellow. *p < 0.05, **p < 0.01, ***p < 0.001, ****p < 0.0001; ns, not significant. Scale bars: 30 μm

of sprouting following SL237 treatment. In contrast, neither p53/p21/p27 OE nor roscovitine treatment were able to fully rescue the lack of sprouting in *vegfc* and *flt4* mutants, suggesting that an additional pathway activated downstream of Vegfc/Flt4 is required to induce dorsal migration and sprout elongation. As the sprouting cells migrate dorsally and pass the anatomical level of the DA, they lose p53, p21, and p27 expression, which results in cell cycle re-entry. In contrast, cells in the ventral side of the PCV, which we have previously show are mostly undifferentiated angioblasts (Nicenboim et al., 2015), perceive low levels of VegfC and lesser ERK activation, impeding CDK inhibitor expression, thereby enabling angioblast proliferation and LEC differentiation.

DISCUSSION

Here, we identify a mechanism-regulating lympho-venous sprouting and differentiation, involving the differential expression of CKIs and controlled progression through the cell cycle. Illuminating different phases of the cell cycle in ECs, through the use of *Tg(fli1a:-Gal4FF;UAS:FUCCI)* embryos, provided valuable insight into the cell cycle dynamics in the developing vasculature. We found that during stages of active lympho-venous budding and sprouting (30–42 hpf) most ECs in the dorsal side of the PCV display mCherry fluorescence, i.e., are in the late-G1 phase of the cell cycle. Moreover, these dorsal PCV cells feature increased expression of p53, p21, and p27, demonstrating a tight correlation between cell-cycle arrest and PCV sprouting. Using CKD inhibitors such as roscovitine or flavopiridol, we also show that halting cell cycle progression in G1 induces hyperangiogenic behaviors that lead to the formation of undifferentiated, ectopic PCV sprouts. These effects, however, were not observed when similar treatments were applied to *p53* mutants, suggesting the specific involvement of p53 in this process. Through the use of EC-specific genetic manipulations, we further demonstrate that PCV ECs overexpressing p53, p27, and p21 acquire an angiogenic phenotype and become more prone to bud off the PCV and sprout. Together, these results indicate that cell autonomous regulation of cell cycle progression in ECs plays essential roles in lympho-venous differentiation, budding, and sprouting.

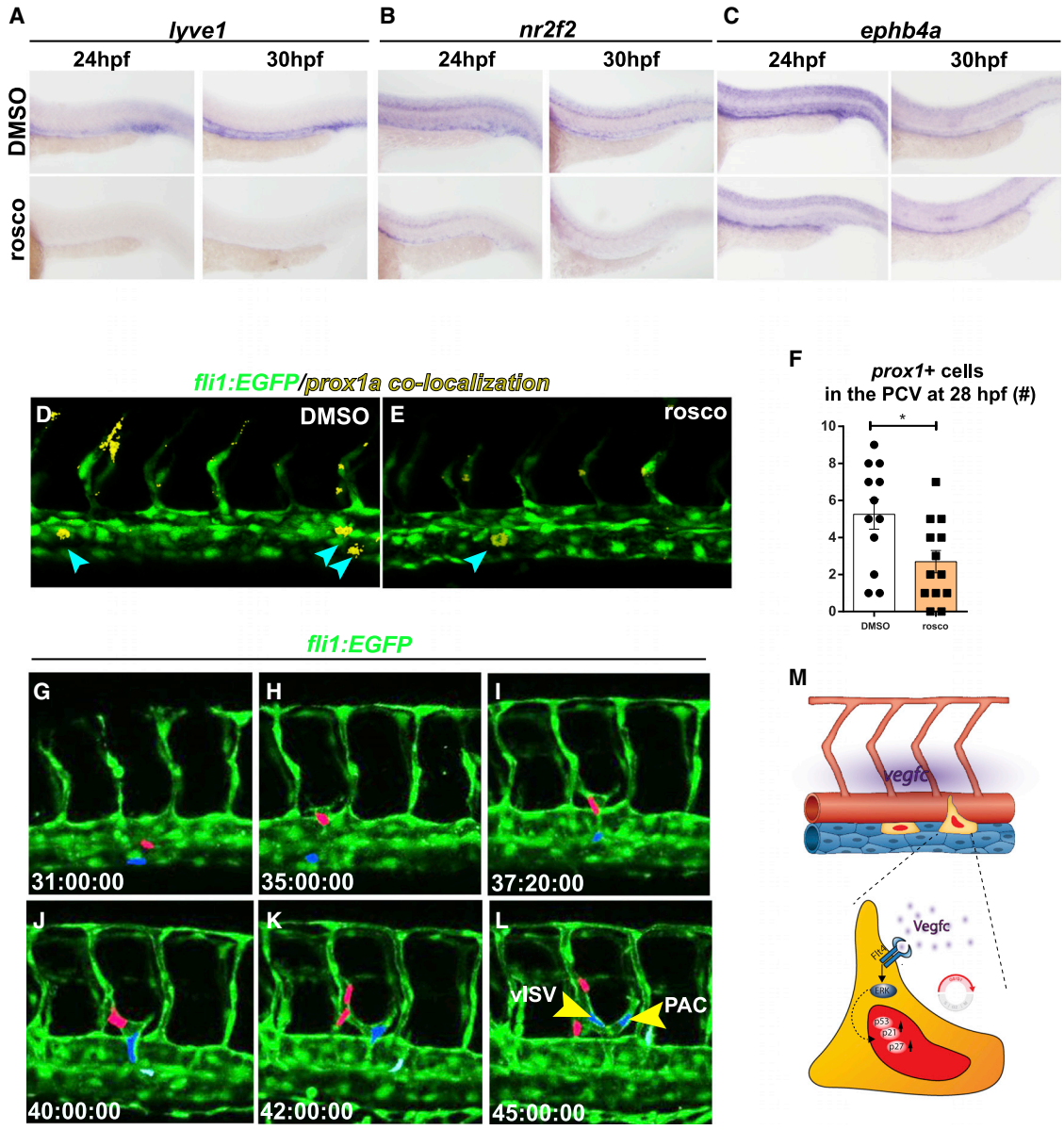

Figure 5. Forced G1 cell-cycle arrest affects lymphatic differentiation

(A–C) *In situ* hybridization at 24 and 30 hpf showing reduced expression of *lyve1* (A) and *nr2f2* (B) following roscovitine treatment. *ephb4a* expression remains unchanged (C).

(D and E) Confocal images of 28-hpf *Tg(fli1:EGFP;prox1a:kalt4:UAS:uncTagRFP)* embryos showing reduced numbers of *prox1*+ cells (light-blue arrowheads) in the PCV upon roscovitine treatment. Co-localization channel is shown in yellow; quantified in (F). Data show mean ± SEM (unpaired t test).

(G–L) Selected images from a time-lapse series depicting the dynamics of PCV sprouting in the presence of roscovitine. Two ECs (colored in red and blue) leave the PCV as part of a single sprout (G) that generates two vessel types. The leading EC (red) connects to an arterial ISV to generate a vISV (I and J); the following cell (blue) divides (J) and gives rise to 2 daughter cells (K and L, yellow arrowheads), with one joining a vISV and the second one incorporating into the nascent PAC.

(M) Schematic model depicting cellular events inducing cell-cycle-arrest-induced sprouting. Dorsal cells of the PCV sense high levels of Vegfc (purple) secreted from the hypocord and the DA. Activation of Vegfr3/Flt4-ERK signaling in these cells leads to cell-cycle-arrest-induced sprouting.

During embryonic development, venous and lymphatic ECs sprout from the PCV in response to Vegfc-Vegfr3 signaling (Semo et al., 2016). Our results indicate that this well-established mitogenic axis in fact induces the expression of p53, p21, and p27 in dorsal PCV ECs to promote their sprouting, as demonstrated by the drastic reduction in p53- and p27-expressing cells in the PCV of *vegfc* and *flt4* mutants. Yet, neither OE of these genes nor roscovitine treatment were able to fully rescue the lack of sprouting in *vegfc* and *flt4* mutants. Despite the increased incidence of angiogenic ECs emerging from the PCV, especially following p53 and p21 OE, these incipient sprouts failed to elongate past the level

of the DA. These results suggest that two different pathways are activated downstream to Vegfc/Flt4, with one driving cell-cycle arrest, which furnishes PCV-ECs with sprouting competence (i.e., the autonomous ability to leave the PCV), and a second one controlling EC migration and sprout elongation. Accordingly, although forcing cell-cycle arrest in *vegfc* and *flt4* mutants resulted in greater numbers of cells emerging from the PCV, it was not sufficient to compensate for the loss of the second arm of the Vegfc/Flt4 pathway, controlling the dorsal migration of the cells.

Downstream to Vegfc-Flt4, ERK was shown to induce both differentiation and sprouting of lymphatic vessels (Deng et al., 2013; Shin et al., 2016). Although ERK phosphorylation plays a pivotal role in diverse cellular functions, including cell proliferation, differentiation, migration, and survival (Mebratu and Tesfaigzi, 2009; Sun et al., 2015), ERK activation can also elicit opposite outcomes, such as cell-cycle arrest and cell death depending on the cellular context (Ebisuya et al., 2005). Previous reports have demonstrated that differences in the duration and magnitude of ERK activity generate variations in signaling output that regulate cell fate decisions (Chen et al., 1999; Ebisuya et al., 2005). In the case of PCV-ECs, activation of the MAPK pathway and ERK phosphorylation are widely regarded as a pro-mitogenic pathway (Simons et al., 2016). Our results, in contrast, suggest that ERK phosphorylation drives sprouting of PCV ECs by inducing cell-cycle arrest. Hence, both roscovitine treatment and EC-specific overexpression of p53 and p21 reverted the inhibition of sprouting exerted by the potent ERK phosphorylation inhibitor SL327. These findings confirm and extend existing evidence that high VEGF signal induces cell-cycle arrest in sprouting tip cells of the mouse retina (Pontes-Quero et al., 2019) by proposing that the sole forced arrest of ECs in G1 phase of the cell cycle can induce initial sprouting and angiogenic behaviors even without ERK signaling.

In addition to activating the ERK-p53/p21 cascade, Vegfc/Flt4 also induced upregulation of p27 in dorsal PCV-ECs. Moreover, p27 expression was strongly downregulated in the absence of active ERK signaling. Yet, p27 OE alone was not sufficient to overcome the effects of ERK inhibition, as opposed to p53/p21 and roscovitine treatment. Based on these results, it seems tempting to speculate that p27 may act downstream to Vegfc/Flt4 but through a parallel, ERK-independent mechanism. Alternatively, a cross-regulatory interaction between p53/p21 and p27 may exist in PCV-ECs, downstream to Vegfc/Flt4.

Finally, it is important to bear in mind that p53, p21, and p27, which are mainly known for their roles in cell cycle regulation, were also implicated in regulating the epithelial-to-mesenchymal transition (EMT). Although it is widely accepted that cells transiently enter cell-cycle arrest during the course of EMT, details on how the two processes are coupled remain unclear. Notably, angiogenic sprouting, especially during embryonic development, share common attributes with EMT, including expression of many of the same genes in angiogenic ECs (Welch-Reardon et al., 2014) and breakdown of basement membranes. Yet, because ECs retain intercellular junctions and migrate as a connected train of cells rather than as individual cells, the process is better defined as a partial endothelial-to-mesenchymal transition (Welch-Reardon et al., 2015). In the future, it will be interesting to investigate potential interactions between cell-cycle arrest and the induction of EMT-like phenotypes, which could be regulated as well by the Vegfc/Flt4 axis.

Overall, our results uncover a mechanism regulating lymphovenous sprouting and differentiation, whereby a mitogenic signal induces cell-cycle arrest to enable angiogenesis. These findings have important implications for the putative short-term effects of using cell cycle inhibitors in settings of pathological angiogenesis, including cancer.

STAR★METHODS

Detailed methods are provided in the online version of this paper and include the following:

- KEY RESOURCES TABLE
- RESOURCE AVAILABILITY
  - Lead contact
  - Materials availability
  - Data and code availability
- EXPERIMENTAL MODEL AND SUBJECT DETAILS
- METHOD DETAILS
  - Generation of transgenic lines
  - Chemical treatments
  - *In situ* hybridization and immunostaining
  - Microscopy and imaging
- QUANTIFICATION AND STATISTICAL ANALYSIS
  - Image processing
  - Statistical analyses

SUPPLEMENTAL INFORMATION

Supplemental information can be found online at https://doi.org/10.1016/j.celrep.2021.109255.

ACKNOWLEDGMENTS

The authors would like to thank Hila Raviv, Lital Shen, and Dean Robinson (Weizmann Institute, Israel) for technical assistance; S. Ben-Dor (Weizmann Institute, Israel) for bioinformatic analysis; Roy Hofi and Anna Tatarin for superb animal care; G. Brodsky (Weizmann Institute, Israel) for graphic designs. D. Kimelman (University of Washington) for providing the *dual fucci* transgenic line and *dual fucci* plasmid; T. Look (Dana Farber Cancer Institute, Boston) for providing *p53*^{m214k} mutant fish; B. Hogan (University of Melbourne) for providing the *p5E-lyve1* construct; and E. Tzahor (Weizmann Institute) for critical reading of the manuscript. The authors are grateful to all the members of the Yaniv lab for discussion, technical assistance, and continuous support. This work was supported in part by European Research Council (818858) to K.Y.; Binational Science Foundation (2015289) to K.Y. and N.D.L.; NIH/NHLBI (R35HL140017) to N.D.L.; Minerva Foundation (712610) to K.Y.; the H&M Kimmel Inst. for Stem Cell Research to K.Y.; and the Estate of Emile Mimran (SABRA program) to K.Y. I.B. is supported by a Senior Postdoctoral fellowship by the Weizmann Institute of Science. K.Y. is the incumbent of the Enid Barden and Aaron J. Jade Professorial Chair in Vascular Biology.

AUTHOR CONTRIBUTIONS

Conceptualization, A.J.-V. and K.Y.; methodology, A.J.-V., N.M., I.B., and G.H.; investigation, A.J.-V., N.M., I.B., Y.T., D.S., G.H., and M.S.; writing – original draft, A.J.-V. and K.Y.; writing – review & editing, I.B., Y.T., M.S., N.D.L.,

and K.Y.; visualization, A.J.-V., I.B., Y.T., and K.Y.; supervision, K.Y.; funding acquisition, K.Y.

DECLARATION OF INTERESTS

The authors declare no competing interests

Received: June 12, 2020
Revised: March 1, 2021
Accepted: May 24, 2021
Published: June 15, 2021

REFERENCES

Alessi, F., Quarta, S., Savio, M., Riva, F., Rossi, L., Stivala, L.A., Scovassi, A.I., Meijer, L., and Prosperi, E. (1998). The cyclin-dependent kinase inhibitors olomoucine and roscovitine arrest human fibroblasts in G1 phase by specific inhibition of CDK2 kinase activity. Exp. Cell Res. *245*, 8–18.

Berghmans, S., Murphey, R.D., Wienholds, E., Neuberg, D., Kutok, J.L., Fletcher, C.D., Morris, J.P., Liu, T.X., Schulte-Merker, S., Kanki, J.P., et al. (2005). tp53 mutant zebrafish develop malignant peripheral nerve sheath tumors. Proc. Natl. Acad. Sci. USA *102*, 407–412.

Betz, C., Lenard, A., Belting, H.-G., and Affolter, M. (2016). Cell behaviors and dynamics during angiogenesis. Development *143*, 2249–2260.

Bouldin, C.M., and Kimelman, D. (2014). Dual fucci: a new transgenic line for studying the cell cycle from embryos to adults. Zebrafish *11*, 182–183.

Calder, A., Roth-Albin, I., Bhatia, S., Pilquil, C., Lee, J.H., Bhatia, M., Levadoux-Martin, M., McNicol, J., Russell, J., Collins, T., and Draper, J.S. (2013). Lengthened G1 phase indicates differentiation status in human embryonic stem cells. Stem Cells Dev. *22*, 279–295.

Canu, G., Athanasiadis, E., Grandy, R.A., Garcia-Bernardo, J., Strzelecka, P.M., Vallier, L., Ortmann, D., and Cvejic, A. (2020). Analysis of endothelial-to-haematopoietic transition at the single cell level identifies cell cycle regulation as a driver of differentiation. Genome Biol. *21*, 157.

Carlson, B.A., Dubay, M.M., Sausville, E.A., Brizuela, L., and Worland, P.J. (1996). Flavopiridol induces G1 arrest with inhibition of cyclin-dependent kinase (CDK) 2 and CDK4 in human breast carcinoma cells. Cancer Res. *56*, 2973–2978.

Carmeliet, P., Ferreira, V., Breier, G., Pollefeyt, S., Kieckens, L., Gertsenstein, M., Fahrig, M., Vandenhoeck, A., Harpal, K., Eberhardt, C., et al. (1996). Abnormal blood vessel development and lethality in embryos lacking a single VEGF allele. Nature *380*, 435–439.

Chen, D., Heath, V., O'Garra, A., Johnston, J., and McMahon, M. (1999). Sustained activation of the raf-MEK-ERK pathway elicits cytokine unresponsiveness in T cells. J. Immunol. *163*, 5796–5805.

Cohen, B., Tempelhof, H., Raz, T., Oren, R., Nicenboim, J., Bochner, F., Even, R., Jelinski, A., Eilam, R., Ben-Dor, S., et al. (2020). BACH family members regulate angiogenesis and lymphangiogenesis by modulating VEGFC expression. Life Sci. Alliance *3*, e202000666.

Covassin, L., Amigo, J.D., Suzuki, K., Teplyuk, V., Straubhaar, J., and Lawson, N.D. (2006). Global analysis of hematopoietic and vascular endothelial gene expression by tissue specific microarray profiling in zebrafish. Dev. Biol. *299*, 551–562.

Dalton, S. (2015). Linking the Cell Cycle to Cell Fate Decisions. Trends Cell Biol. *25*, 592–600.

Deng, Y., Atri, D., Eichmann, A., and Simons, M. (2013). Endothelial ERK signaling controls lymphatic fate specification. J. Clin. Invest. *123*, 1202–1215.

Ebisuya, M., Kondoh, K., and Nishida, E. (2005). The duration, magnitude and compartmentalization of ERK MAP kinase activity: mechanisms for providing signaling specificity. J. Cell Sci. *118*, 2997–3002.

Fang, J.S., Coon, B.G., Gillis, N., Chen, Z., Qiu, J., Chittenden, T.W., Burt, J.M., Schwartz, M.A., and Hirschi, K.K. (2017). Shear-induced Notch-Cx37-p27 axis arrests endothelial cell cycle to enable arterial specification. Nat. Commun. *8*, 2149.

Ferrara, N., Carver-Moore, K., Chen, H., Dowd, M., Lu, L., O'Shea, K.S., Powell-Braxton, L., Hillan, K.J., and Moore, M.W. (1996). Heterozygous embryonic lethality induced by targeted inactivation of the VEGF gene. Nature *380*, 439–442.

Fukuhara, S., Zhang, J., Yuge, S., Ando, K., Wakayama, Y., Sakaue-Sawano, A., Miyawaki, A., and Mochizuki, N. (2014). Visualizing the cell-cycle progression of endothelial cells in zebrafish. Dev. Biol. *393*, 10–23.

Gancz, D., Raftrey, B.C., Perlmoter, G., Marín-Juez, R., Semo, J., Matsuoka, R.L., Karra, R., Raviv, H., Moshe, N., Addadi, Y., et al. (2019). Distinct origins and molecular mechanisms contribute to lymphatic formation during cardiac growth and regeneration. eLife *8*, e44153.

Geudens, I., Coxam, B., Alt, S., Gebala, V., Vion, A.-C., Meier, K., Rosa, A., and Gerhardt, H. (2019). Artery-vein specification in the zebrafish trunk is pre-patterned by heterogeneous Notch activity and balanced by flow-mediated fine-tuning. Dev. Camb. Engl. *146*,, dev181024.

Gibbs-Bar, L., Tempelhof, H., Ben-Hamo, R., Ely, Y., Brandis, A., Hofi, R., Almog, G., Braun, T., Feldmesser, E., Efroni, S., and Yaniv, K. (2016). Autotaxin-Lysophosphatidic Acid Axis Acts Downstream of Apoprotein B Lipoproteins in Endothelial Cells. Arterioscler. Thromb. Vasc. Biol. *36*, 2058–2067.

Hen, G., Nicenboim, J., Mayseless, O., Asaf, L., Shin, M., Busolin, G., Hofi, R., Almog, G., Tiso, N., Lawson, N.D., and Yaniv, K. (2015). Venous-derived angioblasts generate organ-specific vessels during zebrafish embryonic development. Development *142*, 4266–4278.

Hogan, B.M., Herpers, R., Witte, M., Heloterä, H., Alitalo, K., Duckers, H.J., and Schulte-Merker, S. (2009a). Vegfc/Flt4 signalling is suppressed by Dll4 in developing zebrafish intersegmental arteries. Development *136*, 4001–4009.

Hogan, B.M., Bos, F.L., Bussmann, J., Witte, M., Chi, N.C., Duckers, H.J., and Schulte-Merker, S. (2009b). Ccbe1 is required for embryonic lymphangiogenesis and venous sprouting. Nat. Genet. *41*, 396–398.

Isogai, S., Lawson, N.D., Torrealday, S., Horiguchi, M., and Weinstein, B.M. (2003). Angiogenic network formation in the developing vertebrate trunk. Development *130*, 5281–5290.

Jeltsch, M., Kaipainen, A., Joukov, V., Meng, X., Lakso, M., Rauvala, H., Swartz, M., Fukumura, D., Jain, R.K., and Alitalo, K. (1997). Hyperplasia of lymphatic vessels in VEGF-C transgenic mice. Science *276*, 1423–1425.

Jung, H.M., Castranova, D., Swift, M.R., Pham, V.N., Venero Galanternik, M., Isogai, S., Butler, M.G., Mulligan, T.S., and Weinstein, B.M. (2017). Development of the larval lymphatic system in zebrafish. Development *144*, 2070–2081.

Kaipainen, A., Korhonen, J., Mustonen, T., van Hinsbergh, V.W., Fang, G.H., Dumont, D., Breitman, M., and Alitalo, K. (1995). Expression of the fms-like tyrosine kinase 4 gene becomes restricted to lymphatic endothelium during development. Proc. Natl. Acad. Sci. USA *92*, 3566–3570.

Karkkainen, M.J., Haiko, P., Sainio, K., Partanen, J., Taipale, J., Petrova, T.V., Jeltsch, M., Jackson, D.G., Talikka, M., Rauvala, H., et al. (2004). Vascular endothelial growth factor C is required for sprouting of the first lymphatic vessels from embryonic veins. Nat. Immunol. *5*, 74–80.

Kok, F.O., Shin, M., Ni, C.W., Gupta, A., Grosse, A.S., van Impel, A., Kirchmaier, B.C., Peterson-Maduro, J., Kourkoulis, G., Male, I., et al. (2015). Reverse genetic screening reveals poor correlation between morpholino-induced and mutant phenotypes in zebrafish. Dev. Cell *32*, 97–108.

Koltowska, K., Lagendijk, A.K., Pichol-Thievend, C., Fischer, J.C., Francois, M., Ober, E.A., Yap, A.S., and Hogan, B.M. (2015). Vegfc Regulates Bipotential Precursor Division and Prox1 Expression to Promote Lymphatic Identity in Zebrafish. Cell Rep. *13*, 1828–1841.

Küchler, A.M., Gjini, E., Peterson-Maduro, J., Cancilla, B., Wolburg, H., and Schulte-Merker, S. (2006). Development of the zebrafish lymphatic system requires VEGFC signaling. Curr. Biol. *16*, 1244–1248.

Kwan, K.M., Fujimoto, E., Grabher, C., Mangum, B.D., Hardy, M.E., Campbell, D.S., Parant, J.M., Yost, H.J., Kanki, J.P., and Chien, C.B. (2007). The Tol2kit: a multisite gateway-based construction kit for Tol2 transposon transgenesis constructs. Dev. Dyn. *236*, 3088–3099.

Lawson, N.D., and Weinstein, B.M. (2002). In vivo imaging of embryonic vascular development using transgenic zebrafish. Dev. Biol. *248*, 307–318.

Lee, K.-C., Goh, W.L.P., Xu, M., Kua, N., Lunny, D., Wong, J.S., Coomber, D., Vojtesek, B., Lane, E.B., and Lane, D.P. (2008). Detection of the p53 response in zebrafish embryos using new monoclonal antibodies. Oncogene *27*, 629–640.

Liu, L., Michowski, W., Kolodziejczyk, A., and Sicinski, P. (2019). The cell cycle in stem cell proliferation, pluripotency and differentiation. Nat. Cell Biol. *21*, 1060–1067.

Lu, W., Chen, L., Peng, Y., and Chen, J. (2001). Activation of p53 by roscovitine-mediated suppression of MDM2 expression. Oncogene *20*, 3206–3216.

Mäkinen, T., Jussila, L., Veikkola, T., Karpanen, T., Kettunen, M.I., Pulkkanen, K.J., Kauppinen, R., Jackson, D.G., Kubo, H., Nishikawa, S., et al. (2001). Inhibition of lymphangiogenesis with resulting lymphedema in transgenic mice expressing soluble VEGF receptor-3. Nat. Med. *7*, 199–205.

Marcelo, K.L., Goldie, L.C., and Hirschi, K.K. (2013). Regulation of endothelial cell differentiation and specification. Circ. Res. *112*, 1272–1287.

Masood, R., Cai, J., Zheng, T., Smith, D.L., Hinton, D.R., and Gill, P.S. (2001). Vascular endothelial growth factor (VEGF) is an autocrine growth factor for VEGF receptor-positive human tumors. Blood *98*, 1904–1913.

Matsuoka, R.L., Marass, M., Avdesh, A., Helker, C.S., Maischein, H.-M., Grosse, A.S., Kaur, H., Lawson, N.D., Herzog, W., and Stainier, D.Y. (2016). Radial glia regulate vascular patterning around the developing spinal cord. eLife *5*, e20253.

Mebratu, Y., and Tesfaigzi, Y. (2009). How ERK1/2 activation controls cell proliferation and cell death: Is subcellular localization the answer? Cell Cycle *8*, 1168–1175.

Millauer, B., Shawver, L.K., Plate, K.H., Risau, W., and Ullrich, A. (1994). Glioblastoma growth inhibited in vivo by a dominant-negative Flk-1 mutant. Nature *367*, 576–579.

Mühleder, S., Fernández-Chacón, M., Garcia-Gonzalez, I., and Benedito, R. (2021). Endothelial sprouting, proliferation, or senescence: tipping the balance from physiology to pathology. Cell. Mol. Life Sci. *78*, 1329–1354.

Murphey, R.D., Stern, H.M., Straub, C.T., and Zon, L.I. (2006). A chemical genetic screen for cell cycle inhibitors in zebrafish embryos. Chem. Biol. Drug Des. *68*, 213–219.

Nicenboim, J., Malkinson, G., Lupo, T., Asaf, L., Sela, Y., Mayseless, O., Gibbs-Bar, L., Senderovich, N., Hashimshony, T., Shin, M., et al. (2015). Lymphatic vessels arise from specialized angioblasts within a venous niche. Nature *522*, 56–61.

Okuda, K.S., Astin, J.W., Misa, J.P., Flores, M.V., Crosier, K.E., and Crosier, P.S. (2012). lyve1 expression reveals novel lymphatic vessels and new mechanisms for lymphatic vessel development in zebrafish. Development *139*, 2381–2391.

Pauklin, S., and Vallier, L. (2013). The cell-cycle state of stem cells determines cell fate propensity. Cell *155*, 135–147.

Petrova, T.V., and Koh, G.Y. (2018). Organ-specific lymphatic vasculature: From development to pathophysiology. J. Exp. Med. *215*, 35–49.

Pontes-Quero, S., Fernández-Chacón, M., Luo, W., Lunella, F.F., Casquero-Garcia, V., Garcia-Gonzalez, I., Hermoso, A., Rocha, S.F., Bansal, M., and Benedito, R. (2019). High mitogenic stimulation arrests angiogenesis. Nat. Commun. *10*, 2016.

Ruijtenberg, S., and van den Heuvel, S. (2016). Coordinating cell proliferation and differentiation: Antagonism between cell cycle regulators and cell type-specific gene expression. Cell Cycle *15*, 196–212.

Satyanarayana, A., and Kaldis, P. (2009). Mammalian cell-cycle regulation: several Cdks, numerous cyclins and diverse compensatory mechanisms. Oncogene *28*, 2925–2939.

Semo, J., Nicenboim, J., and Yaniv, K. (2016). Development of the lymphatic system: new questions and paradigms. Development *143*, 924–935.

Senderowicz, A.M. (1999). Flavopiridol: the first cyclin-dependent kinase inhibitor in human clinical trials. Invest. New Drugs *17*, 313–320.

Sherr, C.J., and Roberts, J.M. (1999). CDK inhibitors: positive and negative regulators of G1-phase progression. Genes Dev. *13*, 1501–1512.

Sherr, C.J., and Roberts, J.M. (2004). Living with or without cyclins and cyclin-dependent kinases. Genes Dev. *18*, 2699–2711.

Shin, M., Male, I., Beane, T.J., Villefranc, J.A., Kok, F.O., Zhu, L.J., and Lawson, N.D. (2016). Vegfc acts through ERK to induce sprouting and differentiation of trunk lymphatic progenitors. Development *143*, 3785–3795.

Siekmann, A.F., and Lawson, N.D. (2007). Notch signalling limits angiogenic cell behaviour in developing zebrafish arteries. Nature *445*, 781–784.

Simons, M., Gordon, E., and Claesson-Welsh, L. (2016). Mechanisms and regulation of endothelial VEGF receptor signalling. Nat. Rev. Mol. Cell Biol. *17*, 611–625.

Štětková, M., Growková, K., Fojtík, P., Valčíková, B., Palušová, V., Verlande, A., Jorda, R., Kryštof, V., Hejret, V., Alexiou, P., et al. (2020). CDK9 activity is critical for maintaining MDM4 overexpression in tumor cells. Cell Death Dis. *11*, 754.

Stiewe, T. (2007). The p53 family in differentiation and tumorigenesis. Nat. Rev. Cancer *7*, 165–168.

Sugiyama, M., Sakaue-Sawano, A., Iimura, T., Fukami, K., Kitaguchi, T., Kawakami, K., Okamoto, H., Higashijima, S., and Miyawaki, A. (2009). Illuminating cell-cycle progression in the developing zebrafish embryo. Proc. Natl. Acad. Sci. USA *106*, 20812–20817.

Sun, Y., Liu, W.-Z., Liu, T., Feng, X., Yang, N., and Zhou, H.-F. (2015). Signaling pathway of MAPK/ERK in cell proliferation, differentiation, migration, senescence and apoptosis. J. Recept. Signal Transduct. Res. *35*, 600–604.

Tammela, T., Zarkada, G., Wallgard, E., Murtomäki, A., Suchting, S., Wirzenius, M., Waltari, M., Hellström, M., Schomber, T., Peltonen, R., et al. (2008). Blocking VEGFR-3 suppresses angiogenic sprouting and vascular network formation. Nature *454*, 656–660.

van Impel, A., Zhao, Z., Hermkens, D.M., Roukens, M.G., Fischer, J.C., Peterson-Maduro, J., Duckers, H., Ober, E.A., Ingham, P.W., and Schulte-Merker, S. (2014). Divergence of zebrafish and mouse lymphatic cell fate specification pathways. Development *141*, 1228–1238.

Villefranc, J.A., Nicoli, S., Bentley, K., Jeltsch, M., Zarkada, G., Moore, J.C., Gerhardt, H., Alitalo, K., and Lawson, N.D. (2013). A truncation allele in vascular endothelial growth factor c reveals distinct modes of signaling during lymphatic and vascular development. Development *140*, 1497–1506.

Welch-Reardon, K.M., Ehsan, S.M., Wang, K., Wu, N., Newman, A.C., Romero-Lopez, M., Fong, A.H., George, S.C., Edwards, R.A., and Hughes, C.C.W. (2014). Angiogenic sprouting is regulated by endothelial cell expression of Slug. J. Cell Sci. *127*, 2017–2028.

Welch-Reardon, K.M., Wu, N., and Hughes, C.C. (2015). A role for partial endothelial-mesenchymal transitions in angiogenesis? Arterioscler. Thromb. Vasc. Biol. *35*, 303–308.

Yaniv, K., Isogai, S., Castranova, D., Dye, L., Hitomi, J., and Weinstein, B.M. (2006). Live imaging of lymphatic development in the zebrafish. Nat. Med. *12*, 711–716.

Yu, P., Tung, J.K., and Simons, M. (2014). Lymphatic fate specification: an ERK-controlled transcriptional program. Microvasc. Res. *96*, 10–15.

STAR★METHODS

KEY RESOURCES TABLE

REAGENT or RESOURCE	SOURCE	IDENTIFIER
Antibodies		
Cy5-Streptavidin antibody	Jackson ImmunoResearch Labs	Cat# 016-170-084; RRID:AB_2337245
Goat polyclonal anti-GFP (Biotin)	Abcam	Cat# ab6658; RRID:AB_305631
Peroxidase-AffiniPure Goat polyclonal anti-Rabbit IgG	Jackson ImmunoResearch Labs	Cat# 111-035-144; RRID:AB_2307391
Rabbit polyclonal anti-p27 (C-19)	Santa Cruz Biotechnology	Cat# sc-528; RRID:AB_632129
Rabbit polyclonal anti-Tp53	AnaSpec; EGT Group	Cat# AS-55915; RRID:AB_10720860
Chemicals, peptides, and recombinant proteins		
Aphidicolin	Sigma Aldrich	A0781; CAS:38966-21-1
Etoposide	Sigma Aldrich	E1383; CAS:33419-42-0
Flavopiridol	Enzo Life Sciences	ALX-430-161-M005; CAS:146426-40-6
Nocodazole	Sigma Aldrich	M1404; CAS:31430-18-9
Roscovitine	Santa Cruz Biotechnology	sc-24002A; CAS:186692-46-6
SL327	Sigma Aldrich	S4069 CAS:305350-87-2
Critical commercial assays		
TSA Plus Cyanine 3 (TSA Cy3) detection kit	Perkin Elmer	SAT704A001EA
Experimental models: Organisms/strains		
Zebrafish *flt4*$^{um203/um203}$: um203	Kok et al., 2015	ZFIN: ZDB-ALT-160721-30
Zebrafish *Tg(fli1:DsRed)*^{um13}: um13Tg	Hen et al., 2015	ZFIN: ZDB-ALT-100525-3
Zebrafish *Tg(fli1:EGFP)*^{y1}: y1Tg	Lawson and Weinstein, 2002	ZFIN: ZDB-GENO-011017-4
Zebrafish *Tg(fli1a:Gal4FF)*^{ubs3};*Tg(UAS:Kaede)*^{rk8}: ubs3Tg; rk8Tg	Nicenboim et al., 2015	ZFIN: ZDB-FISH-150902-1
Zebrafish *Tg(kdrl:tagBFP)*^{mu293}: mu293Tg	Matsuoka et al., 2016	ZFIN: ZDB-ALT-170119-12
Zebrafish *Tg(lyve1b:dsRed2)*^{nz101}: nz101Tg	Okuda et al., 2012	ZFIN: ZDB-ALT-120723-3
Zebrafish *Tg(mrc1a:EGFP)*^{y251}: y251Tg	Jung et al., 2017	ZFIN: ZDB-ALT-170717-2
Zebrafish *TgBAC(prox1a:KalT4-UAS:uncTagRFP)*^{nim5}: nim5Tg	Nicenboim et al., 2015	ZFIN: ZDB-ALT-140521-3
Zebrafish *tp53*$^{m214k/m214k}$: zdf1	Berghmans et al., 2005	ZFIN: ZDB-ALT-050428-2
Zebrafish *vegfc*$^{um18/um18}$: um18	Villefranc et al., 2013	ZFIN: ZDB-ALT-130718-3
Recombinant DNA		
-3.5ubb:Cerulean-gmnn-2A-mCherry-cdt1	Bouldin and Kimelman, 2014	ZFIN: ZDB-TGCONSTRCT-151028-3
UAS:Cerulian-zGeminin-2A-Cherry-zCdt1Pa	This paper	N/A
p5E-lyve1	Okuda et al., 2012	ZFIN: ZDB-GENE-030131-9516
lyve1:nEGFPpA	This paper	N/A
lyve1:p53-EGFPpA	This paper	N/A
lyve1:p27-EGFPpA	This paper	N/A
lyve1:p21-EGFPpA	This paper	N/A
Software and algorithms		
ImageJ	NIH	https://imagej.nih.gov/ij/; RRID:SCR_003070
Imaris	Bitplane	http://www.bitplane.com/imaris/imaris; RRID:SCR_007370
GraphPad Prism 6	GraphPad	http://www.graphpad.com; RRID:SCR_002798

RESOURCE AVAILABILITY

Lead contact

Further information and requests for resources and reagents should be directed to and will be fulfilled by the lead contact, Karina Yaniv (karina.yaniv@weizmann.ac.il).

Materials availability

All unique reagents generated in this study are available from the lead contact with a completed materials transfer agreement.

Data and code availability

All data supporting the findings of this study are available within the paper and are available from the lead contact upon request.

EXPERIMENTAL MODEL AND SUBJECT DETAILS

Experiments were conducted with zebrafish embryos between 2-5 dpf. Zebrafish were raised by standard methods and handled according to the guidelines of the Weizmann

Institute Animal Care and Use Committee (Gibbs-Bar et al., 2016). For all imaging, *in situ* hybridization and immunofluorescence staining procedures, embryos were treated with 0.003% phenylthiourea (PTU, Sigma-Aldrich) from 8 hpf to inhibit pigment formation. *Tg(fli1:EGFP)*^{y1} (Lawson and Weinstein, 2002), *Tg(kdrl:tagBFP)*^{mu293} (Matsuoka et al., 2016) *Tg(lyve1b:dsRed2)*^{nz101} (Okuda et al., 2012), *Tg(fli1:dsRed)*^{um13} (Hen et al., 2015), *Tg(fli1a:Gal4FF*^{ubs3}*;UAS:Kaede*^{rk8}*)* (Nicenboim et al., 2015), *tp53*$^{m214k/m214k}$ (Berghmans et al., 2005), *Tg(mrc1a:EGFP)*^{y251} (Jung et al., 2017) *TgBAC(prox1a:KalT4-UAS:uncTagRFP)*^{nim}(Nicenboim et al., 2015), *vegfc*$^{um18/\ um18}$ (Villefranc et al., 2013) and *flt4*$^{um203/um203}$ (Kok et al., 2015) were previously described.

METHOD DETAILS

Generation of transgenic lines

To generate the "*fli:fucci*" transgenic reporter, the ubiquitous promoter in the dual *FUCCI* construct (Bouldin and Kimelman, 2014) was replaced with the UAS sequence.

The *UAS:Cerulian-zGeminin-2A-Cherry-zCdt1Pa* construct was then injected into *Tg(fli1a:Gal4FF)*^{ubs3} embryos at 1-cell stage along with Tol2 transposase mRNA.

We used the following primers to amplify the full-length coding sequences of zebrafish p53, p27 and p21:

p53- 5′-TTCACAGCAATGGCGCAAAACG-3′ and
5′- TGTATCGCAGTTCCCCAAATGACC -3′,
p27- 5′-ATGTCCAATGTTCGCTTGTCT-3′ and
5′- TGTGGGTGTCGGACTCAATG -3′,
p21-5′-CTGATACTGCTCCTGAGGAGATCTGA-3′and
5′-CTACGAGACGAATGCAGCTCCAGACA -3′.

After cloning and sequencing, a Gateway-compatible (Invitrogen) middle entry clone was generated using Gateway BP clonase mediated recombination. The *p53, p27* and *p21* coding sequences were then transferred into a *pDestTol2pA2* vector (Kwan et al., 2007) along with a *p5E-lyve1* fragment (Okuda et al., 2012), using Gateway LR clonase (Invitrogen) mediated reaction. The *lyve1:nEGFPpA* construct was generated by combining the *p5E-lyve1* promoter with nuclear localization signal (nls)-EGFP middle entry (*pME-nEGFP*) and *p3E-pA* constructs. The final *lyve1:nEGFPpA*, *lyve1:p53-EGFPpA, lyve1:p27- EGFPpA and lyve1:p21-EGFPpA* constructs (30pg) were co-injected with *Tol2* transposase mRNA (30pg) into 1-cell stage *Tg(fli1:DsRed)*^{um13} embryos.

Chemical treatments

The following chemicals were dissolved in DMSO and added to the fish water at 20 hpf: roscovitine (Santa Cruz Biotechnology, cat# sc-24002A), 50 μM; flavopiridole (Murphey et al., 2006) (Enzo life sciences, ALX-430-161-M005), 5nM; etoposide (Murphey et al., 2006) (Sigma Aldrich, E1383), 1000 μM; nocodazole (Murphey et al., 2006) (Sigma, M1404), 300nM; aphidicoline (Stiewe, 2007) (Sigma, A0781), 297 μM; SL327 (Sigma, S4069), 15 μM (Shin et al., 2016). Controls were incubated with 0.1% DMSO.

In situ hybridization and immunostaining

In situ hybridization was performed as described (Nicenboim et al., 2015). The following primers were used to generate the corresponding riboprobes:

flt4: 5′-TGGAGTTTCTGGCATCTCGT-3′, 5′-ACCATCCCACTGTCTGTCTG-3′

vegfc: 5′-ATGCACTTATTTGGATTTTCTGTCTTCT-3′,
5′- GTCCAGTCTTCCCCAGTATG-3′
lyve1: 5′- AGACGTGGGTGAAATCCAAG -3′,
5′- GATGATGTTGCTGCATGTCC-3′
ephB4a: 5′-CGAACTCTACCTGACGAAGATGA-3′,
5′-CGACAGACCAAAGTCGGACA-3′
p21: 5′-CTAGGCGGAGTCTTTTCGGG -3′,5′-CCACTAGACGCTTCTTGGCT-3′
nr2f2 (Nicenboim et al., 2015).

For detection of p53 and p27 embryos were fixed overnight in 4% PFA, washed in methanol, incubated 1 hr. in 3% H2O2 on ice, and stored in methanol at −20C. For p27 immunostaining, embryos were incubated in 150 mM Tris-HCl at pH 9.0 for 5 min, heated at 70C for 15 min and permeabilized in cold acetone at −20C for 20 min. For p53 staining, embryos were digested with 50mg/ul PK followed by 20 min PFA fixation. For both antibodies, embryos were washed in blocking solution containing 0.1% Triton X-100, 0.1% tween, 1% bovine serum albumin and 10% goat serum for 3hrs. at 4C, and incubated with αp53 (55915s, Anaspec, 1:300) or αp27 (sc-528, Santa Cruz, 1:200) antibodies, along with αGFP-biotin (ab6658, Abcam, 1:300) for 3 days at 4C. Samples were then washed with maleic buffer (150mM maleic acid, 100mM NaCl, 0.1% Tween20, pH 7.4), blocked in maleic buffer containing 2% blocking reagent (Roche, 11-096176-001), and incubated with goat anti-rabbit IgG–horseradish peroxidase (Jackson 1:500) for 2.5 days at 4C for TSA signal amplification, followed by 3 hr. incubation with TSA Plus Cyanine 3 reaction (SAT704A001EA, Perkin Elmer). P-ERK immunostaining was performed as previously described (Shin et al., 2016). To recover the endogenous GFP signal, embryos were incubated in 1:300 streptavidin (Jackson, cat # 016-480-084) for 30 min in RT.

Microscopy and imaging

Live imaging was performed using Zeiss LSM780 or LSM700 upright confocal microscopes (Carl Zeiss, Jena, Germany) equipped with a water immersed X20 NA 1.0 objective lens. Fluorescent proteins were excited sequentially with single-photon lasers (488nm, 561nm). For time-lapse imaging embryos were held in an imaging chamber containing egg water supplemented with tricaine 0.016% (100 mg/25 mL in fish water) to inhibit movement, and with PTU (0.002%) to prevent pigment development. Embryos held this way maintained heartbeat and robust circulation throughout the imaging period (up to 50 hours). Z stacks were acquired at 2.5 μm increments, every 10 min, in 160-170 planes per stack. 2D-, or 3D-reconstructions of image data were prepared using ImageJ (NIH) or Imaris (Bitplane).

QUANTIFICATION AND STATISTICAL ANALYSIS

Image processing

Images were processed offline using ImageJ (NIH) or Imaris (Bitplane). For 3D colocalization analyses in ECs a new colocalization channel was created using the Imaris ‘Colocalization Module’. Co-localization thresholds were set manually. The images shown in this study are single-view, 2D-reconstructions, of collected z series stacks.

Statistical analyses

Comparison of two samples was done using unpaired two-tailed Student’s t test assuming equal variances from at least three independent experiments, unless stated otherwise. Statistical significance for three or more samples was calculated via oneway ANOVA followed by Tukey’s or Dunnett’s multiple comparisons test, unless stated otherwise. All data are reported as mean values ± SEM and were analyzed using Prism 6 software (GraphPad Software, Incorporated, La Jolla, CA, USA).